Analytical prediction of the linear and nonlinear behaviour of steel beams rehabilitated using FRP sheets

M.A. Youssef*

Department of Civil and Environmental Engineering, The University of Western Ontario, London, ON, CANADA, N6A 5B9

Abstract

The importance to rehabilitate ageing and deteriorated existing steel structures has motivated researchers to develop simple and efficient rehabilitation techniques. One of the currently developed techniques involves bonding Fibre Reinforced Plastic (FRP) sheets to the flanges of steel beams. This paper presents an analytical model to predict the linear and nonlinear behaviour of steel beams rehabilitated using this technique. The model is based on the solution of the differential equations governing the composite behaviour of a rehabilitated steel beam and includes representation of the peel and shear behaviour of the adhesive material. A bending test was conducted on a W-shaped steel beam, with glass FRP sheets bonded to its flanges, and the experimental results were used to validate the model. The model predictions for the failure load, failure mechanism, midspan deflection, steel strains, and FRP strains were found to be in excellent agreement with the experimental results. The model was also used to predict some parameters that were difficult to evaluate experimentally. This provided a better understanding of the behaviour of the rehabilitated beam.

Keywords: Rehabilitation; Steel Beam; FRP Sheet; Analytical Model; Adhesive Stress; Failure Load.

* Corresponding author. Tel. +1-519-661-2111 Ext. 88661; fax: 1-519-661-3779.
E-mail address: myoussef@eng.uwo.ca (M.A. Youssef)

1. Introduction

In the past two decades, FRP sheets had been extensively used to rehabilitate concrete structures [1, 2]. This allowed increasing the strength and/or ductility of these structures while benefiting from the FRP material advantages including: ease of application, high strength-to-weight ratio, and excellent resistance against corrosion and chemical attacks. New uses of FRP sheets to upgrade the resistance of steel structures have recently been studied. Sen et al. [3] tested six steel beams after bonding carbon FRP sheets to their bottom flange. A considerable increase in the capacity of composite beams was reported. Miller et al. [4] used carbon FRP sheets to strengthen four steel bridge girders. The experimental results indicated that the stiffness of the rehabilitated girders increased by 10% to 37%. EL Damatty et al. [5] investigated experimentally and analytically the flexural capacity of a W-shaped beam with glass FRP sheets bonded to its flanges. The excellent performance of the beam encouraged them to analytically assess the effect of bonding glass FRP sheet to the bottom flange of an existing composite steel bridge. They concluded that a 38 mm glass FRP sheet would increase the truck loading capacity of the bridge by 25% [6]. To gain better understanding of the behaviour of the steel beams rehabilitated using FRP sheets, EL Damatty et al. [5] presented a closed form analytical model to predict the stresses induced in the adhesive and the FRP sheets. Disadvantages of this analytical approach included its inability to predict the behaviour of the rehabilitated beam after yielding and to capture the peeling behaviour of the adhesive.

The current study provides an analytical model that describes the linear and nonlinear composite behaviour of steel/FRP beams. The model is based on the solution of the differential equations governing the behaviour and takes into account the shear and peel behaviour of the adhesive material. A steel beam rehabilitated by bonding glass FRP sheets to its flanges is tested to validate the model predictions. The following sections of the paper describe the tested specimen, the analytical model, and the experimental and analytical results.

2. Experimental Work

A simply supported W150x37 steel beam, strengthened by bonding 19 mm glass FRP sheets to its top and bottom flanges, was tested experimentally to provide the necessary results to validate the analytical model. Fig. 1 gives a schematic of the test setup. It shows that the composite beam had a span, L, of 2800 mm. It also shows that the FRP sheets were centred on the beam and had a length, L_f, of 2400 mm. The FRP sheets width was 152 mm, matching the steel beam width. The steel and plastic materials were bonded using 0.79 mm thick methacrylate adhesive system. This adhesive was chosen as it provides the best level of bond between steel and glass FRP sheets [7]. The method, for bonding the FRP sheets to the steel beam, was similar to that explained by El Damatty et al. [5].

The yield stress, modulus of elasticity, and strain-hardening ratio of the steel beam were 400 MPa, $2x10^5$ MPa, and 0.01, respectively. The used FRP sheets were manufactured using the pultrusion process and consisted mainly of large number unidirectional layers that provided strength and stiffness in the longitudinal direction. The tensile strength, compressive strength, and modulus of elasticity of these sheets, as experimentally evaluated by the manufacturer, were 135 MPa, 165 MPa, and $12.4x10^3$ MPa, respectively. Considering the adhesive, El Damatty and Abushagur [7] evaluated experimentally its shear and peel strength as 21.79 MPa, and 4 N/mm, respectively. They also reported the average values for the constants of the linear continuous springs simulating the shear and peel stiffness of this adhesive as K_s=21.79 N/mm^3 and K_p=2.26 N/mm^3, respectively

The load was transferred to the test specimen through a rigid load distributor at the two points shown in Fig. 1. A load-controlled manner with a rate of 2.0 kN/minute and a displacement-controlled manner with a rate of 0.5 mm/minute were used for the elastic and the plastic ranges, respectively. An LVDT, attached to the midspan section of the tested beam, was used to measure the vertical displacement. In addition, four strain gauges, attached to the outer face of the FRP sheets and the inner faces of the steel beam flanges at midspan section, were used to measure the strain values.

3. Analytical Model

A typical simply supported steel beam, strengthened by bonding FRP sheets to its top and bottom flanges, is shown in Fig. 1. An infinitesimal element of the bottom FRP sheet, located at distance x from the midspan section, is shown in Fig. 2. In this figure, u_1 and u_2 are the axial displacements of the edge of the steel beam and the FRP sheet, respectively. u_1 is expected to be higher than u_2 because of the flexibility of the adhesive material.

In this section, the equations used to represent the steel beam behaviour are first introduced. This is followed by the derivation of the differential equations governing the shear and peel behaviour of the adhesive material. Finally, the solutions of these differential equations are presented.

3.1 Behaviour of the steel beam

For any steel section, the relationship between the steel beam moment, M_s, and the axial strain at its edge, $\frac{du_1}{dx}$, can be determined by conducting a sectional analysis. This relationship can be approximated to a bilinear curve similar to that shown in Fig. 3 and the values defining this curve can be evaluated. These values are:

M_p: yielding moment.

ε_p: edge axial strain corresponding to M_p.

K_1: elastic stiffness.

K_2: post-elastic stiffness.

Using these values, the relationship between M_s and $\frac{du_1}{dx}$ can be written as:

Elastic stage ($\frac{du_1}{dx} \le \varepsilon_p$): $$M_s = K_1 . \frac{du_1}{dx} \quad (1a)$$

Plastic stage ($\frac{du_1}{dx} \ge \varepsilon_p$): $$M_s = M_p + K_2 (\frac{du_1}{dx} - \varepsilon_p) \quad (1b)$$

3.2 Differential equation governing the shear behaviour of the adhesive material

The shear stress, τ, developing in the adhesive can be expressed by the following equation:

$$\tau = K_s(u_1 - u_2) \quad (2)$$

Where K_s is the spring constant simulating the shear stiffness of the adhesive.

From the equilibrium of the horizontal forces shown in Fig. 2, the following differential equation can be written.

$$u_1 = u_2 - \frac{t_f.E_f}{K_s}\frac{d^2u_2}{dx^2} \quad (3)$$

Where E_f and t_f are the modulus of elasticity and the thickness of the FRP sheet, respectively.

Differentiating equation (3) with respect to x and setting $\nu = \frac{du_2}{dx}$ will result in the following differential equation that relates the axial strain of the extreme fibres of the steel section and that of the FRP sheet (ν).

$$\frac{du_1}{dx} = \nu - \frac{t_f.E_f}{K_s}\nu'' \quad (4)$$

The external moment (M) acting on the rehabilitated section is equal to sum of the internal moment in the steel section (M_s) and moment resulting from the axial stresses in the FRP sheets (M_{FRP}) and can be written as:

$$M = M_s + M_{FRP} = M_s + b(h + t_f)E_f.t_f.\nu \quad (5)$$

Where b and h are the width of the FRP section and the height of steel section, respectively.

Simplifying equations 1, 4 and 5 results in the following differential equations that governs the shear behaviour of the adhesive material:

Elastic stage ($\frac{du_1}{dx} \le \varepsilon_p$): $$\frac{K_s.M}{K_1.E_f.t_f} = w_E^2\nu - \nu'' \quad (6a)$$

Plastic stage ($\frac{du_1}{dx} \ge \varepsilon_p$): $$\frac{K_s.(M - M_p + K_2.\varepsilon_p)}{K_2.E_f.t_f} = w_p^2\nu - \nu'' \quad (6b)$$

Where:

$$w_E^2 = \frac{K_s}{E_f.t_f} + \frac{K_s.b.(h + t_f)}{K_1} \quad (7a)$$

$$w_P^2 = \frac{K_s}{E_f.t_f} + \frac{K_s.b.(h + t_f)}{K_2} \quad (7b)$$

3.3. Differential equation governing the peel behaviour of the adhesive material

The equations resulting from the equilibrium of vertical forces and moments shown in Fig. 2 are:

$$\frac{dV_f}{dx} = -K_p.w.b \quad (8)$$

$$V_f = \frac{dM_f}{dx} + \frac{b.t_f}{2}.\tau \quad (9)$$

Where:

V_f and M_f: shear force and moment in the FRP sheet.

w: adhesive peel displacement.

K_p: spring constant simulating the peel stiffness of the adhesive.

Applying the moment-curvature relationship, equation 10, and coupling equations 8 and 9 will result in the differential equation governing the peel behaviour (equation 11).

$$M_f = E_f.I_f \frac{d^2w}{dx^2} \quad (10)$$

$$\frac{d^4w}{dx^4} + \lambda^4 w = \frac{b.t_f^2}{2.I_f} \nu'' \quad (11)$$

Where, I_f is the inertia of the FRP sheet and

$$\lambda^4 = \frac{K_P.b}{E_f.I_f} \quad (12)$$

3.4 Solution in the elastic loading stage:

In this stage, the rehabilitated length of the beam can be divided in two zones, zone AE with x varying from zero to 0.5 L_p, and zone BE with x varying from 0.5 L_p to 0.5 L_f (x is measured from the beam midspan and L_p is the distance between the two concentrated loads acting on the beam). The main difference between the two zones is the applied moment as it is constant in zone AE and varying in zone BE.

- Zone AE: $0 \le x \le 0.5\ L_p$

The moment in this region is constant and can be written as:

$$M_{AE} = M_o = \frac{P}{2}(L - L_p) \tag{13}$$

The solutions of the differential equations 6a and 11 can be written as:

$$\nu_{AE} = A_1.\sinh(w_E.x) + B_1.\cosh(w_E.x) + \frac{K_s M_o}{K_1.E_f.t_f.w_E^2} \tag{14}$$

$$\begin{aligned} w_{AE} &= A_3\cos(\lambda.x)\cosh(\lambda.x) + B_3\cos(\lambda.x)\sinh(\lambda.x) + C_3\sin(\lambda.x)\cosh(\lambda.x) \\ &+ D_3\sin(\lambda.x)\sinh(\lambda.x) + \frac{b.t_f^2.w_E^2}{2.I_f.(\lambda^4 + w_E^4)}\left[A_1\sinh(\omega_E x) + B_1\cosh(\omega_E x)\right] \end{aligned} \tag{15}$$

- Zone BE: $0.5\ L_p \le x \le 0.5\ L_f$

The moment in this region can be written as a function of the constant moment M_o in zone AE.

$$M_{BE} = \frac{2.M_o.(0.5L - x)}{(L - L_p)} \tag{16}$$

The solutions of the differential equations 6a and 11 can be written as:

$$\nu_{BE} = C_1.\sinh(w_E.x) + D_1.\cosh(w_E.x) + \frac{K_s(M_{BE})}{K_1.E_f.t_f.w_E^2} \tag{17}$$

$$\begin{aligned} w_{BE} &= E_3\cos(\lambda.x)\cosh(\lambda.x) + F_3\cos(\lambda.x)\sinh(\lambda.x) + G_3\sin(\lambda.x)\cosh(\lambda.x) \\ &+ H_3\sin(\lambda.x)\sinh(\lambda.x) + \frac{b.t_f^2.w_E^2}{2.I_f.(\lambda^4 + w_E^4)}\left[C_1\sinh(\omega_E x) + D_1\cosh(\omega_E x)\right] \end{aligned} \tag{18}$$

From the symmetry of the problem, it can be noted that the constants A1, B_3 and C_3 are equal to zero. The constants B_1, C_1, D_1 A_3, D_3, E_3, F_3, G_3, and H_3 can be evaluated by applying the following boundary conditions.

$$\begin{aligned}
&\nu_{AE} = \nu_{BE} && \text{at} \quad x = \frac{L_P}{2} && \text{(Continuity of strains)} \\
&\frac{d\nu_{AE}}{dx} = \frac{d\nu_{BE}}{dx} && \text{at} \quad x = \frac{L_P}{2} && \text{(Continuity of curvature)} \\
&\nu_{BE} = 0 && \text{at} \quad x = \frac{L_f}{2} && \text{(FRP strain is zero at its edges)}
\end{aligned} \tag{19a}$$

$$\begin{aligned}
&w_{AE} = w_{BE} && \text{at } x = \frac{L_p}{2} && \text{(Continuity of displacement)} \\
&\frac{dw_{AE}}{dx} = \frac{dw_{BE}}{dx} && \text{at } x = \frac{L_p}{2} && \text{(Continuity of rotation)} \\
&\frac{d^2 w_{CE}}{dx^2} = 0 && \text{at } x = \frac{L_f}{2} && \text{(FRP moment is zero at its edges)} \\
&(V_f)_{CE} = 0 && \text{at } x = \frac{L_f}{2} && \text{(FRP shear is zero at its edges)} \\
&(M_f)_{AE} = (M_f)_{BE} && \text{at } x = \frac{L_p}{2} && \text{(Continuity of moment)} \\
&(V_f)_{AE} = (V_f)_{BE} && \text{at } x = \frac{L_p}{2} && \text{(Continuity of shear)}
\end{aligned} \tag{19b}$$

3.5 Solution in the plastic loading stage:

In this stage, the rehabilitated length of the beam can be divided in three zones, zone AP with x varying from zero to 0.5 L_p, zone BP with x varying from 0.5 L_p to x_p, and zone CP with x varying from x_p to 0.5 L_f.

Where x_p is the distance from the beam midspan to the section at which M_s=M_p.

- Zone AP: $x \leq 0.5\ L_p$ (Applied moment > M_p)

  The moment in this region will be equal to M_o and the differential equations governing the behaviour are equations 6b and 11. The solutions of these equations can be written in the form:

$$\nu_{AP} = A_2.\sinh(w_p.x) + B_2.\cosh(w_p.x) + \frac{K_s(M_o - K_1.\varepsilon_p + K_2.\varepsilon_p)}{K_2.E_f.t_f.w_p^2} \quad (20)$$

$$w_{AP} = A_4\cos(\lambda.x)\cosh(\lambda.x) + B_4\cos(\lambda.x)\sinh(\lambda.x) + C_4\sin(\lambda.x)\cosh(\lambda.x)$$
$$+ D_4\sin(\lambda.x)\sinh(\lambda.x) + \frac{b.t_f^2.w_p^2}{2.I_f.(\lambda^4 + w_p^4)}\left[A_2\sinh(\omega_p x) + B_2\cosh(\omega_p x)\right] \quad (21)$$

- Zone BP: $0.5\,L_p \le x \le x_p$ (Moment $\ge M_p$)

The moment in this zone is similar to that given by equation 16. The solutions of equation 6b and 11 are:

$$\nu_{BP} = C_2.\sinh(w_p.x) + D_2.\cosh(w_p.x) + \frac{K_s(M_{BP} - K_1.\varepsilon_p + K_2.\varepsilon_p)}{K_2.E_f.t_f.w_p^2} \quad (22)$$

$$w_{BP} = E_4\cos(\lambda.x)\cosh(\lambda.x) + F_4\cos(\lambda.x)\sinh(\lambda.x) + G_4\sin(\lambda.x)\cosh(\lambda.x)$$
$$+ H_4\sin(\lambda.x)\sinh(\lambda.x) + \frac{b.t_f^2.w_p^2}{2.I_f.(\lambda^4 + w_p^4)}\left[C_2\sinh(\omega_p x) + D_2\cosh(\omega_p x)\right] \quad (23)$$

- Zone CP: $x_p \le x \le 0.5\,L_f$ (Moment $\le M_p$)

This zone is similar to zone BE and the equations defining the behaviour in this zone are:

$$\nu_{CP} = E_2.\sinh(w_E.x) + F_2.\cosh(w_E.x) + \frac{K_s(M_{CP})}{K_1.E_f.t_f.w_E^2} \quad (24)$$

$$w_{CP} = I_4\cos(\lambda.x)\cosh(\lambda.x) + J_4\cos(\lambda.x)\sinh(\lambda.x) + K_4\sin(\lambda.x)\cosh(\lambda.x)$$
$$+ L_4\sin(\lambda.x)\sinh(\lambda.x) + \frac{b.t_f^2.w_E^2}{2.I_f.(\lambda^4 + w_E^4)}\left[E_2\sinh(\omega_E x) + F_2\cosh(\omega_E x)\right] \quad (25)$$

From the symmetry of the problem, the constants B_4 and C_4 are equal to zero. The methodology used to determine x_p, and the constants A_2, B_2, C_2, D_2, E_2, F_2, A_4, D_4, E_4, F_4, G_4, H_4, I_4, J_4, K_4, and L_4 is as follows:

1. A suitable value for x_p is assumed.
2. The six boundary equations given by equation (26) are solved for A_2, B_2, C_2, D_2, E_2, and F_2.

$$\frac{d\nu_{AP}}{dx} = 0 \qquad \text{at} \quad x = 0 \qquad \text{(Symmetry of the problem)}$$

$$\nu_{AP} = \nu_{BP} \qquad \text{at} \quad x = \frac{L_P}{2} \qquad \text{(Continuity of strains)}$$

$$\nu_{BP} = \nu_{CP} \qquad \text{at} \quad x = x_p \qquad \text{(Continuity of strains)}$$

$$\frac{d\nu_{AP}}{dx} = \frac{d\nu_{BP}}{dx} \qquad \text{at} \quad x = \frac{L_P}{2} \qquad \text{(Continuity of curvature)} \qquad (26)$$

$$\frac{d\nu_{BP}}{dx} = \frac{d\nu_{CP}}{dx} \qquad \text{at} \quad x = x_p \qquad \text{(Continuity of curvature)}$$

$$\nu_{CP} = 0 \qquad \text{at} \quad x = \frac{L_f}{2} \qquad \text{(FRP stress is zero at its edges)}$$

3. Equation 4 is applied to evaluate two values for $\frac{du_1}{dx}$ at $x=x_p$. The first value is evaluated using ν_{BP} (equation 22) and the second value is evaluated using ν_{CP} (equation 24).

4. If the difference between the two values evaluated in step 3 is greater than a predefined tolerance, then the assumed x_p is incorrect and steps 1 through 4 have to be repeated.

5. The remaining constants are evaluated by applying the following ten boundary conditions:

$$w_{AP} = w_{BP} \qquad \text{at} \quad x = \frac{L_p}{2} \qquad \text{(Continuity of displacement)}$$

$$w_{BP} = w_{CP} \qquad \text{at} \quad x = x_p \qquad \text{(Continuity of displacement)}$$

$$\frac{dw_{AP}}{dx} = \frac{dw_{BP}}{dx} \qquad \text{at} \quad x = \frac{L_p}{2} \qquad \text{(Continuity of rotation)}$$

$$\frac{dw_{BP}}{dx} = \frac{dw_{CP}}{dx} \qquad \text{at} \quad x = x_p \qquad \text{(Continuity of rotation)} \qquad (27)$$

$$\frac{d^2 w_{CP}}{dx^2} = 0 \qquad \text{at} \quad x = \frac{L_f}{2} \qquad \text{(FRP moment is zero at its edges)}$$

$$(V_f)_{CP} = 0 \qquad \text{at} \quad x = \frac{L_f}{2} \qquad \text{(FRP shear is zero at its edges)}$$

$$(M_f)_{AP} = (M_f)_{BP} \qquad \text{at} \quad x = \frac{L_p}{2} \qquad \text{(Continuity of moment)}$$

$$(M_f)_{BP} = (M_f)_{CP} \qquad \text{at} \quad x = x_p \qquad \text{(Continuity of moment)}$$

$$(V_f)_{AP} = (V_f)_{BP} \qquad \text{at} \quad x = \frac{L_p}{2} \qquad \text{(Continuity of shear)}$$

$$(V_f)_{BP} = (V_f)_{CP} \qquad \text{at} \quad x = x_p \qquad \text{(Continuity of shear)}$$

4. Experimental and Analytical Results:

The experimentally tested beam was analyzed using the analytical model explained in section 3. Observations on its behaviour and comparisons between the analytical and the experimental results are given in the following sections.

4.1 Analytical behaviour of the tested steel beam

The steel beam was analyzed using sectional analysis. The resulting relationship between the moment in the steel beam and the extreme fibre strains is shown in Fig. 4. In the same figure, the bilinear approximation is shown. The following values defines the bilinear curve:

$$\begin{aligned} M_P &= 120.00\ \text{kN.m.} \\ \varepsilon_P &= 0.002189 \\ \frac{K_2}{K_1} &= 0.005993 \end{aligned} \qquad (28)$$

4.2 Analytical Prediction of the plastic load P_p

The following steps were conducted to evaluate the load P_p causing the moment in the steel beam to reach M_p (120.00 kN.m.):

1. W_E was calculated using equation (7a) and the value of K_1 evaluated in section 4.1.
2. A value for the applied load P was assumed and the constants B1, C1, and D1 were evaluated by solving equations (19a).
3. The strain in the FRP sheet at midspan section (x=0) was evaluated using equation (14).
4. Knowing the total applied moment (M), the steel beam moment (M_s) could be evaluated using equation (5).
5. P_p was calculated by proportion ($P_p = P_{assumed}\ M_p/M_s$). For the tested beam, P_p was found to be 143.07 kN. This means that the glass FRP sheet increased the load required to reach the plastic moment (120.00 kN.m.) from 128.57 kN to 143.07 kN (11.28% increase).

4.3. Analytical behaviour at P_b (143.07 kN):

In this section, the behaviour of the rehabilitated beam was studied analytically at a load of 143.07 kN. This load represents the end of the linear stage as discussed in section 4.2. The constants of equations (14, 15, 17, 18) were first evaluated at P_b by solving equations (19a, 19b). A discussion of the beam behaviour at this load is given below.

1. The distribution of the axial strains in the FRP sheet along the beam length was evaluated using equations (14) and (17). Multiplying these strains by E_f resulted in the axial stress distribution shown in Fig. 5. Axial stresses were increasing from zero at the FRP sheet edge to a maximum value of 25.63 MPa (18.99% of the FRP sheet tensile strength) at the midspan section.
2. The moment carried by the FRP sheet was calculated using their evaluated axial stresses (step 2). This allowed calculating the moment carried by the steel beam using equation (5). Figure 6 shows the total applied moment. It also shows the portion of the moment carried by the FRP sheet and that carried by the steel section. The total applied moment was having a trapezoidal distribution with a maximum value, M_{LT}=133.53 kN.m. The FRP sheet contribution in carrying this moment was increasing from zero at its edge to a maximum value of 14.27 kN.m (10.7% of M_{LT}) at the midspan section.
3. Equation (3) was applied to obtain the relative displacement (u_1-u_2) that occurs between the FRP sheet and steel section. Multiplying this relative displacement by K_s led to an evaluation of the shear stresses developing in the adhesive. The distribution of these stresses is shown in Fig. 7. The maximum value of the adhesive shear stress was at the edges of the FRP sheet and was equal to 7.65% of the adhesive expected shear capacity
4. The adhesive peel displacements were evaluated using equations (15), and (18). Multiplying these values by K_p resulted in the distribution of the adhesive peel stresses shown in Fig. 8. The peel strength, obtained by El Damatty and Abushagur (2003) through a standard ASTM D1878 test, was presented as force per unit length. The corresponding acting peel force could be obtained by integrating the peel stresses within the length at which separation tends to

occur. Integrating the peel stresses, shown in Fig. 8, at the FRP sheet edge, showed that the adhesive peel stress reached 29.88% of its expected capacity.

5. The moment and shear in the FRP sheet, Figs. 9, and 10, were evaluated using equations (9) and (10). Their extreme values were found near the edges of the FRP sheet. The maximum combined axial/flexural stress in the FRP sheet occurred at a distance 462 mm from the beam midspan and was equal to 25.664 MPa (19.01% of the FRP sheet Tensile Strength). This shows that at this loading level, the flexural stresses resulted in an increase of 0.13% in the FRP sheet stresses. The maximum shear stress in the FRP sheet was 1.14 MPa.

4.4 Failure load

The following incremental analysis was conducted to analytically predict the failure load:

1. The initial load and the step number, n, were set equal to P_b and one, respectively.
2. A suitable load increment dP was chosen.
3. x_p and the constants of equations (20, 21, 22, 23, 24, 25) were evaluated at a load equal to $P_b + n\ dP$ using the iterative method given in section 3.5.
4. Equations (3, 20, 22, 24) were applied to obtain the relative displacements (u_1-u_2) that occur between the FRP sheet and steel section. Multiplying the maximum relative displacement by K_s led to an evaluation of the maximum shear stress developing in the adhesive. This stress was compared with the shear strength of the adhesive material to judge if adhesive shear failure would occur at this load level.
5. The adhesive peel displacements were evaluated using equations (21, 23, 25). Multiplying these values by K_p results in the distribution of the adhesive peel stresses. The corresponding acting peel force could be obtained by integrating the peel stresses within the length at which separation tends to occur. This force was compared with the peel strength of the adhesive material to judge if adhesive peel failure would occur at this load level.
6. The distribution of the axial strains in the FRP sheet along the beam length was evaluated using equations (20, 22, 24). Multiplying these strains by E_f resulted in the axial stresses in

the FRP sheet. The moment in the FRP sheet was also evaluated using equation (10). The maximum value for the combined axial and flexural stresses were calculated and compared with the adhesive tensile strength to judge if FRP sheet tensile failure would occur at this load level.

7. Steps 3 through 6 were repeated until failure occurred.

Using these steps, the analytical model predicted that tensile failure of the FRP bottom sheet initiated the collapse of the specimen. The FRP sheet increased the specimen load capacity from 128.57 kN (load corresponding to M_P) to 206.88 kN (61% increase). The observed experimental failure load (216.47 kN) was in close agreement with that predicted analytically. Following is a discussion of the behaviour of the tested specimen at failure.

1. Figure 11 shows the relationship between the location of the plastic hinge and the applied load. The bonding of the FRP sheet increased the distance over which the steel beam moment reached M_p from 933.33 mm (distance between applied loads) to 1350.17 mm (44.66% increase).
2. The distribution of the axial stresses in the FRP sheet is shown in Fig. 5. These stresses are increasing from zero at the FRP sheet edge to a maximum value of 132.73 MPa (96.18% of the FRP sheet tensile strength) at the midspan section. The rate of increase of these axial stresses at the FRP sheet edges started to significantly increase at the plastic hinge location. This led to the adhesive shear stresses distribution shown in Fig. 7. At failure, the adhesive shear stresses reached 32.25% of its ultimate capacity.
3. Figure 12 shows the total applied moment. It also shows the portion of the moment carried by the FRP sheet and that carried by the steel section. The total moment was having a maximum value, M_{NT}=193.08 kN.m. The FRP sheet contribution in carrying this moment was increasing from zero at its edge to a maximum value of 70.29 kN.m (36.4% of M_{NT}) at the midspan section.
4. Figure 8 shows the distribution of the adhesive peel stresses. Integrating the peel stresses showed that the adhesive peel stress reached 37.00% of its expected capacity.

5. The moment and shear in the FRP sheet are shown in Figs. 9 and 10, respectively. The maximum moment occurred at the point of the applied load and was equal to 0.05 kN.m. The maximum combined axial/flexural stress occurred near the applied load and was equal to 135 MPa. This explained the experimentally observed tensile failure of the FRP sheet, shown in Fig. 13, where failure occurred near the concentrated load.

4.5 Experimental and analytical strains at the midspan section:

This section reports the results of the four strain gauges installed at the midspan section as well as the strains evaluated analytically. The load-strain curves in the steel beam and the FRP sheet are given in Figs. 14 and 15, respectively. Examining the two figures can draw the following observations.

1. The analytical model was able to predict the steel and the FRP sheet strains in both the linear and nonlinear ranges of loading with high accuracy.
2. The differences between the absolute values of the strains measured in the top and bottom flanges, and the top and bottom FRP sheets were minor. This verifies the accuracy of these strain measurements.
3. The analytical load-strain curves show a linear behaviour up to a load of 143.07 kN (moment of 133.53 kN.m.). At this load, the steel section moment reached its M_p value (120.00 kN.m.). This indicates that bonding the FRP sheets to the steel flanges increased the load required to reach M_p from 128.57 kN to 143.07 kN (increase of 11.3%).

4.6. Experimental and analytical load-deflection relationship

In this section, the load-deflection diagram was obtained analytically and compared to that obtained experimentally. For each load increment, the calculated strains in the flanges of the steel beam were used to evaluate the curvature distribution along the member length. These curvatures were then integrated to evaluate the vertical deflection at the beam midspan. The analytical predictions as well as the experimental results are shown in Fig. 16. The figure shows that the

analytical predictions for the linear and nonlinear deflections are in close agreement with the experimental ones. The analytical load-deflection curve was linear up to a load of 143.07 kN (Moment = 120.00 kN.m). Beyond this load value, the figure indicates that the section possessed a positive stiffness (10.43% of the initial stiffness) and had the ability to carry extra loads. This stiffness resulted only from the contribution of the FRP plates.

5. Conclusions

In this paper, an analytical model capable of predicting the linear and nonlinear behaviour of steel beams rehabilitated using FRP sheets is developed. This model can be used to predict the strains, and stresses in the steel beam, the FRP sheet, and the adhesive material. It can also predict the deformations of the rehabilitated beam up to failure. The following failure modes are included in the model: adhesive shear failure, adhesive peel failure, and FRP sheet tensile failure. To validate the model predictions, a steel beam rehabilitated using glass FRP sheets was experimentally tested. The model predictions for the midspan strains and deflections and for the failure load were compared against the experimental results. In general, the comparison between the experimental, and analytical results showed excellent agreement. The tested specimen failed when the FRP sheet reached its maximum tensile strength. This failure mode was confirmed analytically and it was found analytically that the point of maximum combined flexural and axial stresses was located near the location of the applied load.

Acknowledgements

The author would like to acknowledge the financial support provided to this project by the Natural Sciences and Engineering Research Council of Canada (NSERC), and the University of Western Ontario.

References

[1] Malek AM, Saadatmanesh H, Ehsani MR. Prediction of failure load of R/C beams strengthened with FRP plate due to stress concentration at the plate end. ACI Struct J 1998; 95(2): 142-52.

[2] Sause R, Harries KA, Walkup SL, Pessiki S, Ricles JM. Flexural behavior of concrete columns retrofitted with carbon fiber-reinforced polymer jackets. ACI Struct J 2004; 101(5): 708-16.

[3] Sen R, Liby L, Mullins G. Strengthening steel bridge sections using CFRP laminates. Compos Part B-Eng 2001; 32(4): 309-22.

[4] Miller TC, Chajes MJ, Mertz DR, Hastings, JN. Strengthening of a steel bridge girder using CFRP plates. J Bridge Eng-ASCE 2001; 6(6): 514-22.

[5] El Damatty AA, Abushagur M, Youssef MA. Experimental and analytical investigation of steel beams rehabilitated using GFRP sheets. Steel Compos Struct 2003; 3(6): 421-38.

[6] El Damatty AA, Abushagur M, Youssef, MA. Rehabilitation of composite steel bridges using GFRP plates. Appl Compos Mater 2005; 12(5): 309-25.

[7] El Damatty AA, Abushagur M. Testing and modeling of shear and peel behavior for bonded steel/FRP connections. Thin Wall Struct 2003; 41(11): 987-1003.

List of figures

Fig. 1. Rehabilitated steel beam.

Fig. 2. Stresses, forces, and moments acting on an infinitesimal element of the FRP sheet**.**

Fig. 3. Variation of the steel section moment with the extreme fibres axial strain.

Fig. 4. Variation of steel section moment with the extreme fibres axial strain for the tested steel beam.

Fig. 5. Relationship between FRP sheet axial stresses and the distance from midspan at M_p and at failure.

Fig. 6. Relationship between the moment and the distance from midspan at M_p.

Fig. 7. Relationship between the adhesive shear stress and the distance from midspan at M_p and at failure.

Fig. 8. Relationship between the adhesive peel stress and the distance from midspan at M_p and at failure.

Fig. 9. Relationship between the moment in the FRP sheet and the distance from midspan at M_p and at failure.

Fig. 10. Relationship between the shear in the FRP sheet and the distance from midspan at M_p and at failure.

Fig. 11. Relationship between the applied load and its distance to the plastic hinge (x_p-0.5 L_p).

Fig. 12. Relationship between the moment and the distance from midspan at failure.

Fig. 13. Failure mechanism of the rehabilitated beam.

Fig. 14. Relationship between the applied load (P) and the strains in the steel beam at midspan section.

Fig. 15. Relationship between the applied load (P) and the strains in the FRP sheets at midspan section.

Fig. 16. Relationship between applied load and midspan deflection of the rehabilitated steel beam.

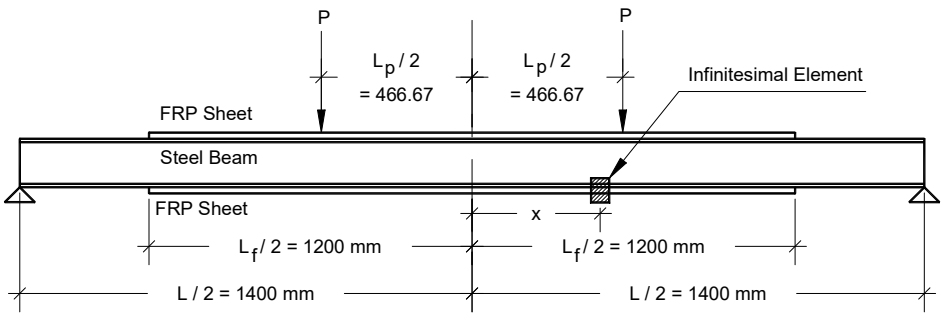

Fig. 1. Rehabilitated steel beam.

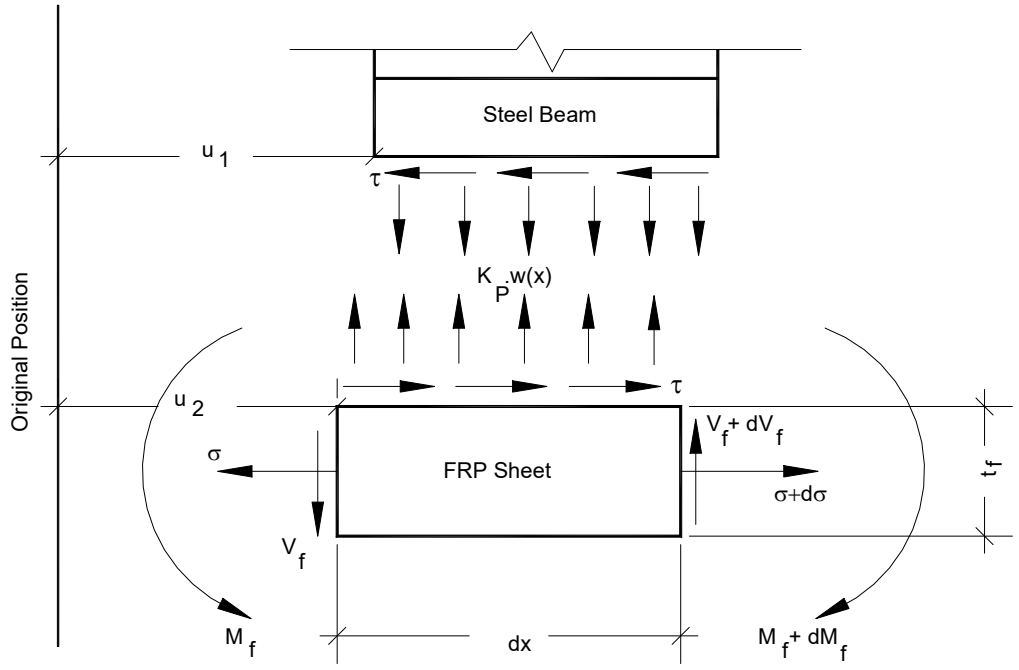

Fig. 2. Stresses, forces, and moments acting on an infinitesimal element of the FRP sheet.

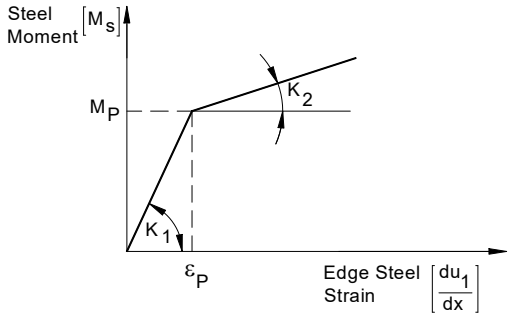

Fig. 3. Variation of the steel section moment with the extreme fibres axial strain.

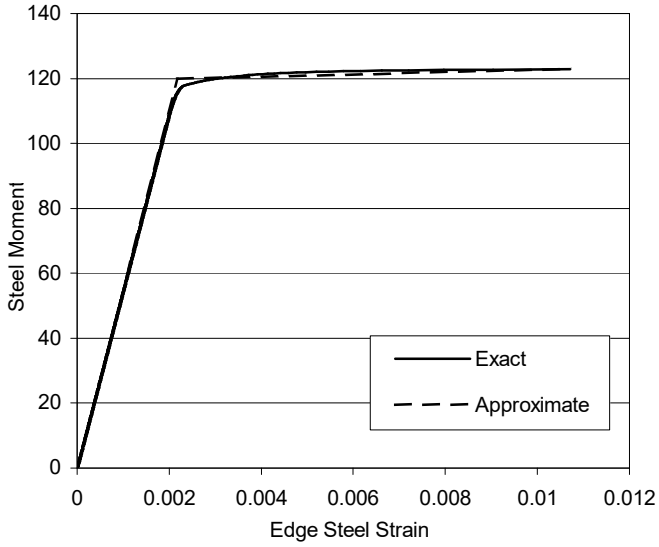

Fig. 4. Variation of steel section moment with the extreme fibres axial strain for the tested steel beam.

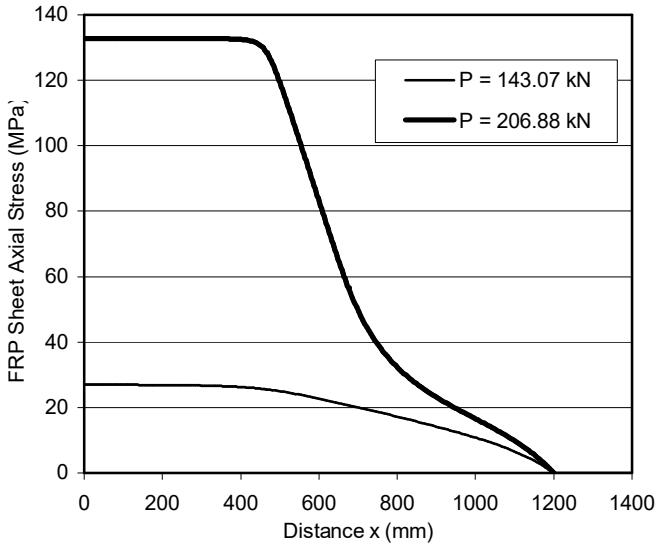

Fig. 5. Relationship between FRP sheet axial stresses and the distance from midspan at M_p and at failure.

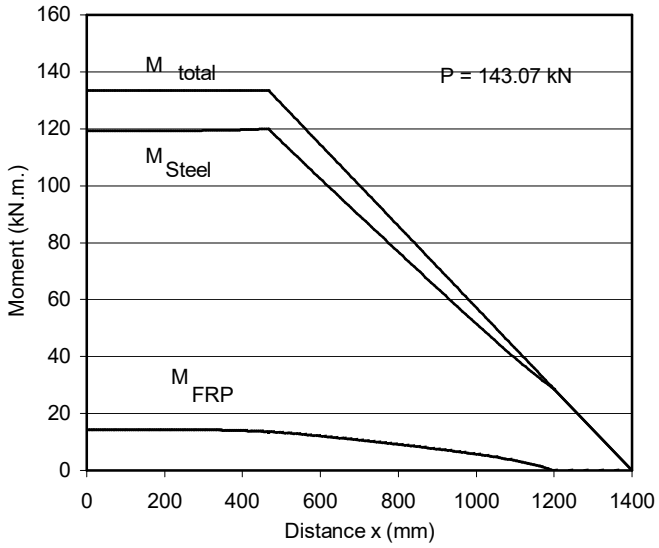

Fig. 6. Relationship between the moment and the distance from midspan at M_p.

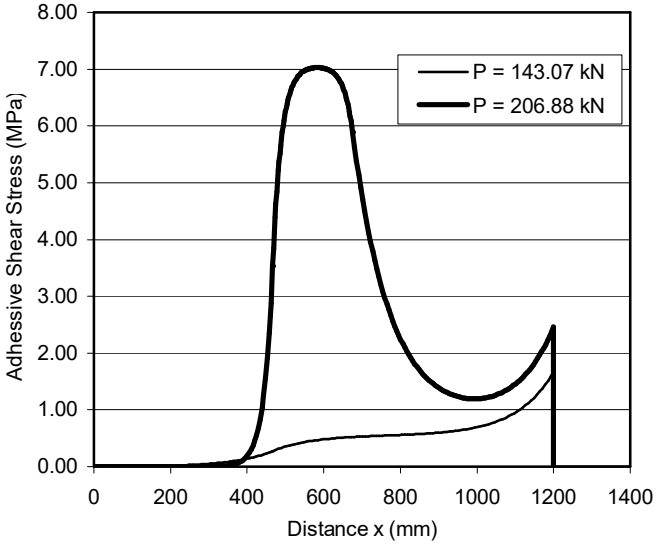

Fig. 7. Relationship between the adhesive shear stress and the distance from midspan at M_p and at failure.

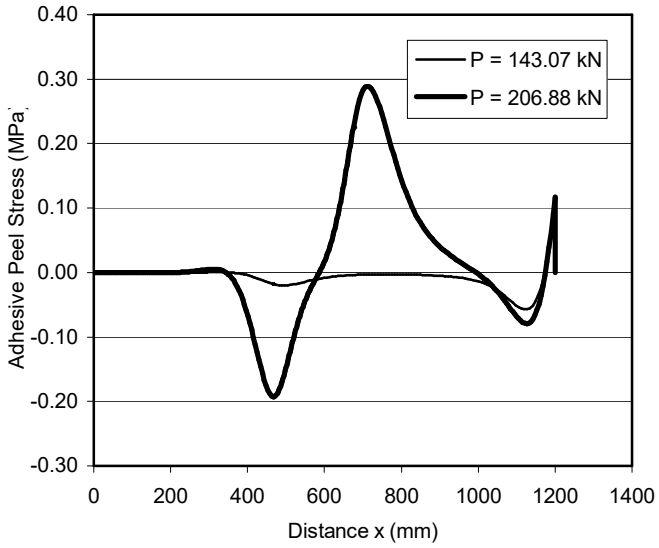

Fig. 8. Relationship between the adhesive peel stress and the distance from midspan at M_p and at failure.

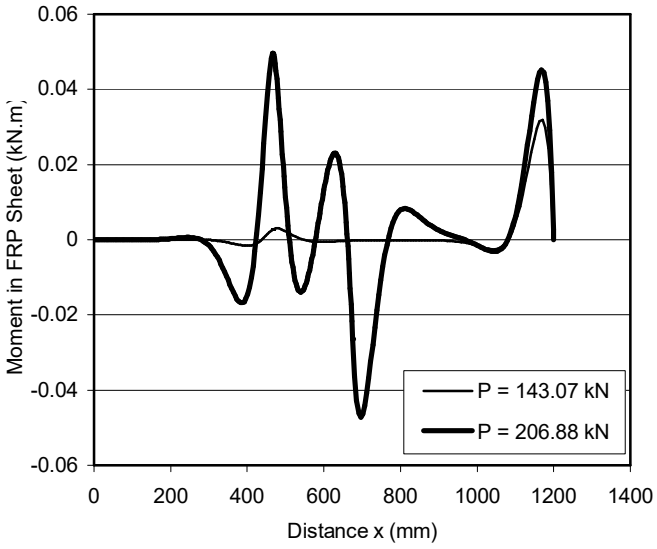

Fig. 9. Relationship between the moment in the FRP sheet and the distance from midspan at M_p and at failure.

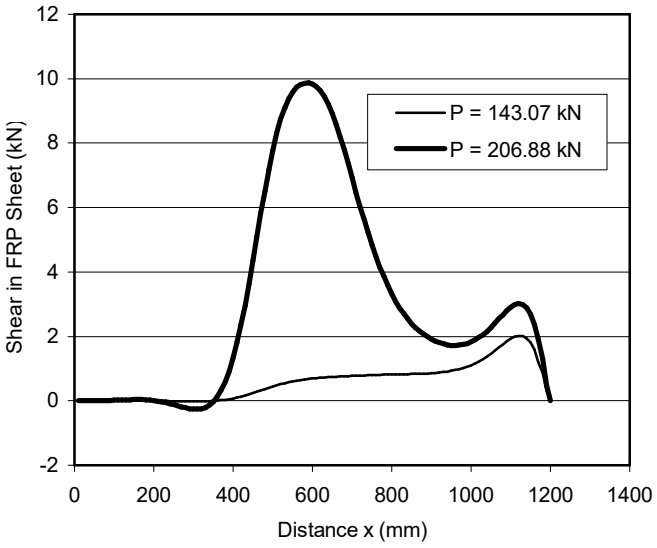

Fig. 10. Relationship between the shear in the FRP sheet and the distance from midspan at M_p and at failure.

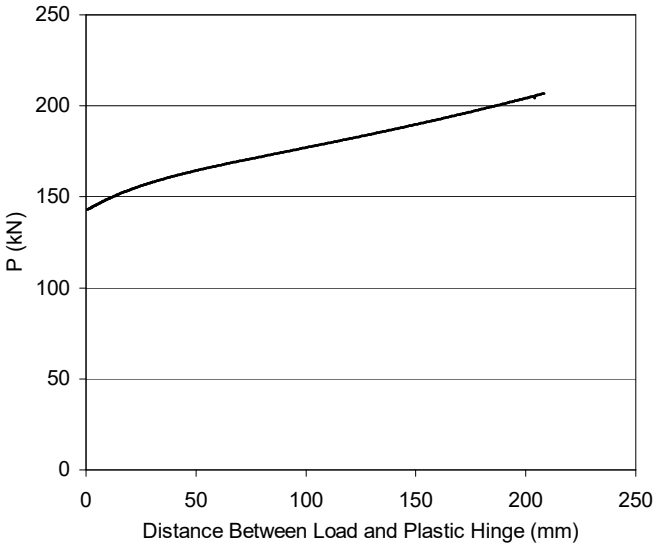

Fig. 11. Relationship between the applied load and its distance to the plastic hinge (x_p-0.5 L_p).

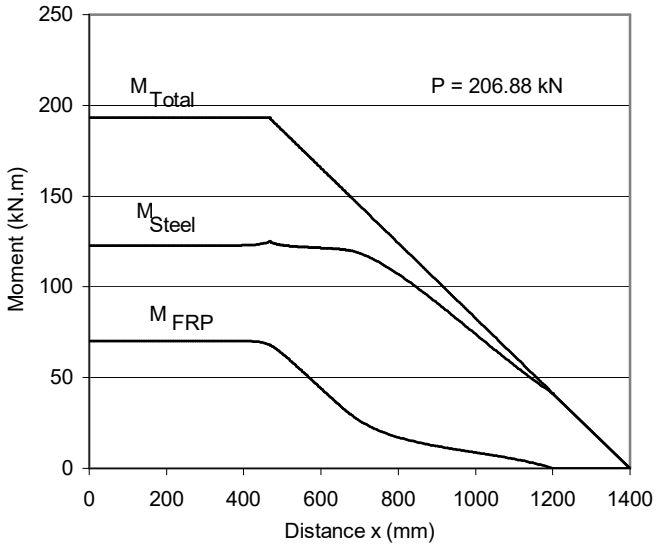

Fig. 12. Relationship between the moment and the distance from midspan at failure.

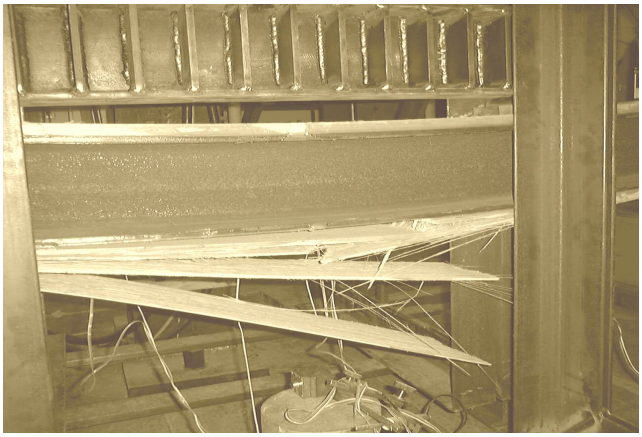

Fig. 13. Failure mechanism of the rehabilitated beam.

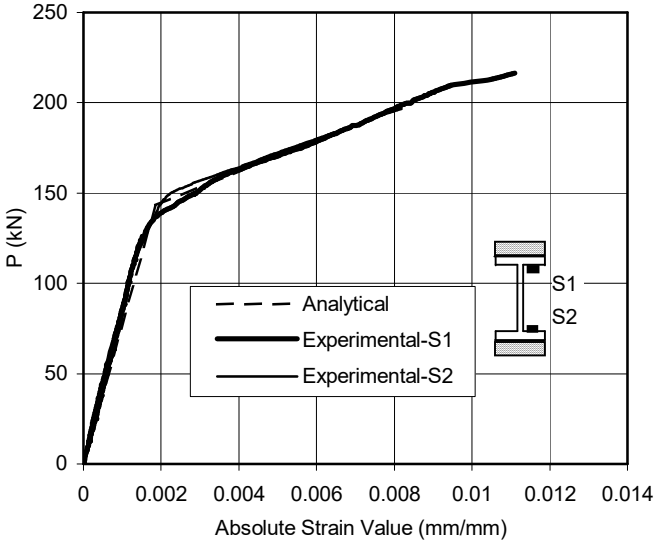

Fig. 14. Relationship between the applied load (P) and the strains in the steel beam at midspan section.

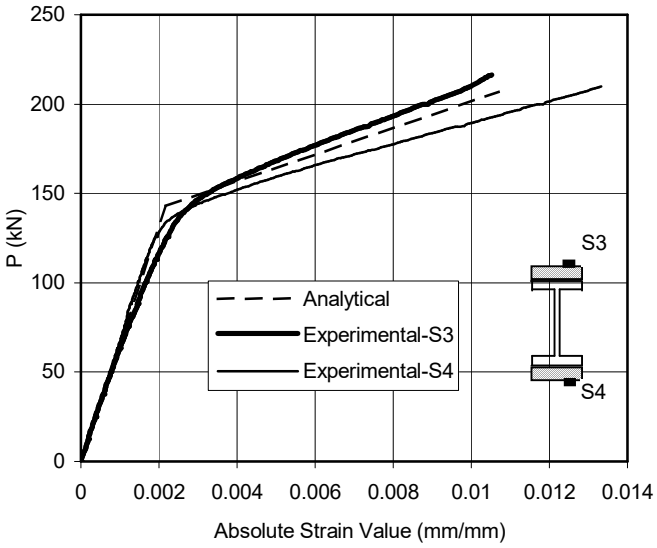

Fig. 15. Relationship between the applied load (P) and the strains in the FRP sheets at midspan section.

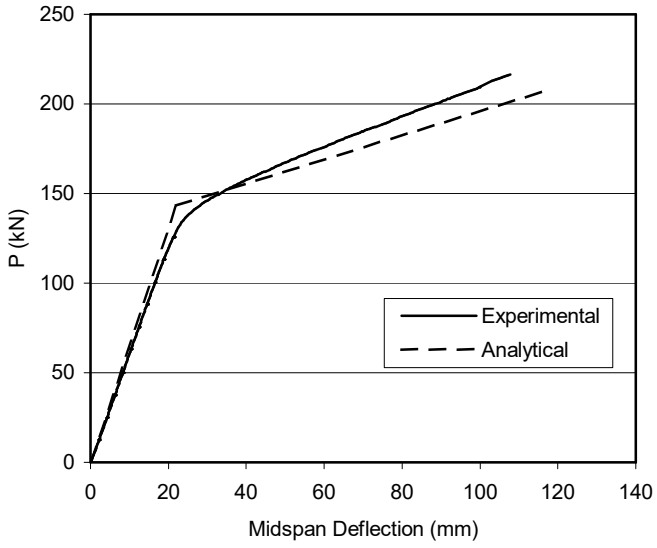

Fig. 16. Relationship between applied load and midspan deflection of the rehabilitated steel beam.